The Astrophysical Journal, 370:144–157, 1991 March 20

RELICS OF AN ERUPTIVE STARBURST IN NGC 1569

William H. Waller[1]
Five College Astronomy Department, University of Massachusetts, Amherst; and Astronomy Department, University of Washington, Seattle
Received 1990 May 16; accepted 1990 August 1

ABSTRACT

Hα, *R*, and *I* band CCD images of the "posteruptive" irregular galaxy NGC 1569 are presented. The discovery of two arclike structures of diffuse Hα emission located more than 1 kpc beyond the star-forming bar is reported. These features are used to estimate an age for the near-nuclear starburst that created them along with other filamentary and armlike structures previously seen in Hα photographs. Considerations of likely outflow geometries and kinematics lead to an estimated age range of 10–60 Myr, in rough accord with the 10–20 Myr age that Israel and de Bruyn derive based on considerations of synchrotron losses in the nonthermal radio spectrum.

The gravitational and kinematic energies associated with the Hα arcs are estimated to be orders of magnitude higher than can be provided by a single supernova explosion. Coherent outbursts involving thousands of supernovae each could explain the diffuse Hα features without exceeding the starbirth rate inferred from the total Hα luminosity of the galaxy.

Comparisons between the line and continuum imagery show the inner bar to be populated with H II regions of high Hα equivalent width and blue color. These regions are located on opposite sides of the brightest continuum emission which, in turn, is offset from the dynamical nucleus as defined by the outer *B* and *V* isophotes. A starburst history incorporating these observations is proposed and discussed.

Subject headings: galaxies: evolution — galaxies: individual (NGC 1569) — galaxies: interstellar matter — galaxies: stellar content — galaxies: structure

I. INTRODUCTION

NGC 1569 (VII Zw 16, Arp 210) is a Magellanic-type irregular galaxy located in a relativity nearby and uncrowded part of the M81/IC 342/Maffei grouping of galaxies (Tully and Fisher 1987). Its unusual Hα emitting morphology prompted Zwicky (1971) to classify it as a "post-eruptive system similar to M82." Since then, NGC 1569 has been the subject of many observational studies involving photographic imagery of the Hα filaments (Hodge 1974), Fabry-Perot interferometry of the Hα velocity field (de Vaucouleurs, de Vaucouleurs, and Pence 1974; de Vaucouleurs 1981), aperture synthesis mapping of the radio continuum emission (Seaquist and Bignell 1976; Condon 1983; Israel and de Bruyn 1988). 21 cm mapping of the H I emission (Reakes 1980; Israel and van Driel 1990), 2.6 mm observations of the ^{12}CO emission (Young, Gallagher, and Hunter 1984), and UV–IR photometry of the starlight (see literature review by W. van Driel as presented by Israel 1988).

The picture that has emerged is of a small, relatively nearby irregular galaxy, rich in H I, poor in metals, extremely bright at Hα, and very blue in broad-band colors. Despite its low mass, it has recently undergone a strong burst of star formation, whose repurcussions are evident throughout the electromagnetic spectrum. The burst appears to have produced a bipolar outflow of ionized gas that is directed perpendicular to the highly inclined disk (de Vaucouleurs, de Vaucouleurs, and Pence 1974). Such intense activity from a relatively unevolved system in many ways mimics the global starbursts that are thought to have characterized the beginnings of earlier type galaxies such as the Milky Way and M31 (Sandage 1986). Therefore, the ability to study the NGC 1569 starburst at close range represents a valuable opportunity to better understand the early stages of galaxy evolution and perhaps to better diagnose the "primordial" galaxies that are just now becoming detectable at high redshift.

In this paper, I present further evidence for a major starburst having erupted 10–60 Myr ago from the nucleus of NGC 1569. The evidence is in the form of Hα-emitting arcs of ionized gas, whose displacement from the bursting center are used to estimate the burst age. The most recent high-mass star formation is explored by analyzing the Hα, *R* band, and *I* band imagery. The brightest Hα emission and bluest colors are found to be well matched with one another but significantly displaced from the once-bursting nucleus. The relative displacements, ages, and burst strengths are discussed in the context of the galaxy's recent history.

Table 1 lists the properties of NGC 1569 that are adopted in this paper. As usual, the most controversial property is the distance. The distance that I have adopted is based on the observation of *resolved* blue stars in NGC 1569 that have *B* magnitudes of 20.2 (Ables 1971). By applying a calibration of the absolute magnitude of the brightest blue stars as a function of M_B of the parent galaxy, Arp and Sandage (1985) derive an apparent distance modulus of $(m-M)_B = 29.0 \pm 1.0$ mag (see also Ables 1971 and de Vaucouleurs, de Vaucouleurs, and Pence 1974 who obtain similar results). From multicolor photometry and spectroscopy of the neighboring star BD $+64°450$, Israel (1988) derives a large foreground reddening to the star of $E(B-V) = 0.55$ and to the galaxy of $E(B-V) = 0.56$. This amount of reddening is in good agreement with that obtained from H-line flux measurements of NGC 1569 at Hα (this paper) and Brγ (Waller *et al.* 1991). The resulting extinction-corrected distance modulus is then $(m-M)_0 = 26.7 \pm 0.6$ which corresponds to a distance of 2.2 ± 0.6 Mpc.

[1] Visiting Astronomer, Kitt Peak National Observatory, National Optical Observatories, operated by the Association of Universities for Research in Astronomy, Inc., under contract with the National Science Foundation.

TABLE 1

Adopted Properties of NGC 1569

Property	Adopted Value
Type[a,b]	SmIV/IBm
R.A. (1950)[a]	$04^h26^m05^s$
Decl. (1950)[a]	64°44′24″
Galactic longitude[a]	143°69
Galactic latitude[a]	11°24
Radial velocity (heliocentric)[c]	-77 km s^{-1}
Position angle of major axis[d]	116°
Inclination[d]	63°
$E(B-V)$[e]	0.56 mag
$(B-V)_0$[d,e]	0.23 mag
B_0[d,e]	9.64 mag
Distance[e]	2.2 Mpc
Holmberg radius[b,e]	1′44 (925 pc)
L_0(UV + optical)[e]	$1.2 \times 10^9\ L_\odot$
L(FIR)[e]	$7 \times 10^8\ L_\odot$
M(H I)[c,e]	$11 \times 10^7\ M_\odot$
$M(H_2)$[e,f]	$2 \times 10^7\ M_\odot$
M(dynamic)[c,e]	$33 \times 10^7\ M_\odot$
M_*	$15 \times 10^7\ M_\odot$

[a] Sandage and Tammann 1981 (RSA).
[b] de Vaucouleurs *et al.* 1976 (RC2).
[c] Reakes 1980.
[d] Ables 1971.
[e] Israel 1988 and references therein.
[f] Young *et al.* 1984.

At this distance, the mysterious central objects A and B (first noted by Ables 1971) would have absolute blue magnitudes of -13.3 and -12.5 mag, respectively. By contrast, 30 Doradus has $M_B \approx -10.3$ mag. Therefore, the central objects are either super–star clusters $\sim$5 times more luminous than 30 Doradus (Arp and Sandage 1985) or simply foreground blue stars (Ables 1971). The spatial coincidence between objects A and B and the photometric nucleus (see § III*c*), along with the *composite hot supergiant* spectral classifications for both objects (A2 I + B0 I), and the similarities between the radial velocities of A, B, and the H I centroid of NGC 1569 (Arp and Sandage 1985) provide additional reasons for choosing the resident supercluster interpretation. Any larger distance (e.g., Hunter, Gallagher, and Rautenkranz 1982) would make the clusters even more luminous and difficult to explain. High-resolution imaging and spectroscopy of A and B by the *Hubble Space Telescope* (after its optical aberrations are corrected) should be helpful in pinning down the true properties of these intriguing objects, without confusion from the ambient galaxy light.

The adopted position angle of the major axis and inclination of the disk are based on the outer B and V isophotes as mapped by Ables (1971). The inclination appears as an important ingredient along with the distance when computing the displacements and kinematic ages of the arcs.

All corrections of extinction are based on the "mean" interstellar extinction law, as tabulated by Scheffler (1982), where $A_v = 3.2\ E(B-V)$.

II. OBSERVATIONS AND REDUCTIONS

A summary of the CCD imagery obtained for this study is provided in Table 2. The Hα, R, I, and [S III] band images were obtained at the Cassegrain focus of the Kitt Peak No. 1 0.9 m telescope during clear weather.[3] With the f/7.5 secondary in place, the resolution on the RCA-3 CCD chip is 0″86 pixel^{-1}, and the field of view is approximately 7′3 × 4′5 (see Fig. 1). Care was taken to point the telescope, so that the nearby 10th mag star BD +64°450 would be just north of the field of view and therefore out of harm's way. This meant missing out on imaging the northerly extremities of NGC 1569 as well. However, inspection of the wider field photographic images of Hodge (1974) indicates that very little nebular emission has been missed. The following sections will be concerned with the 3′ × 3′ portion of the image that contains all of the detected Hα emission features.

[3] Kitt Peak National Observatory is operated by the Association of Universities for Research in Astronomy, Inc., under contract with the National Science Foundation.

TABLE 2

Observing Log

A.

Observing Parameter	Value
Telescope	KPNO No. 1 0.9 m @f/7.5
Detector	RCA-3 CCD
Pizel size	0″86
Field of view	7′3 × 4′5
Date	1985 Oct 22

B.

Observing Parameter	Filter			
	Hα	R	I	[S III]
λ_0 (Å)	6563	6500	8290	9540
FWHM (Å)	38	1283	1947	144
Integration time (s)	2400	600	600	2400

Imaging at Hα (see Fig. 1) was conducted using an interference filter (no. 810, λ_0 6563, $\Delta\lambda$38) provided by Kitt Peak. The transmission characteristics of this filter combined with the 1.7 Å blueshift of NGC 1569 results in the transmission of Hα(λ_0 6563) with 0.73 transmissivity, [N II](λ_0 6584) with 0.16 transmissivity, and [N II](λ_0 6548) with 0.46 transmissivity. The net contamination from [N II] is expected to be 10% in emission (Kennicutt and Kent 1983) and 4% in the present imagery. All subsequent Hα fluxes are corrected for this effect.

Imaging at R and I bands was conducted with the Mould R and I filters that are commonly used at Kitt Peak. An attempt was made to image at [S III](λ9532) using a 144 Å bandwidth filter centered on 9540 Å. The resulting image suffered from strong fringing, however, with only the brightest H II region rising sufficiently above the noise for further analysis.

To calibrate the galaxy imagery, image of the sdOp type standard star BD +28°4211 (Stone 1977) were obtained through all filters. Images of an illuminated screen inside the dome were taken through each filter at the beginning of the night for the purpose of flattening the background variations in the galaxy images.

Initial processing of the CCD images—including bias averaging and subtraction, darkframe subtraction, and flat-field averaging and division—was carried out at Kitt Peak using the Mountain Photometry Code package. Further processing—including image arithmetic, median filtering, synthetic aperture photometry, and contouring—was conducted at the University of Washington using the Image Reduction and Analysis Facility (IRAF) software created at Kitt Peak National Observatory. Synthetic aperture photometry on the images of the standard star yielded the following conversions between flux and count rate (after bias subtraction, flat-field

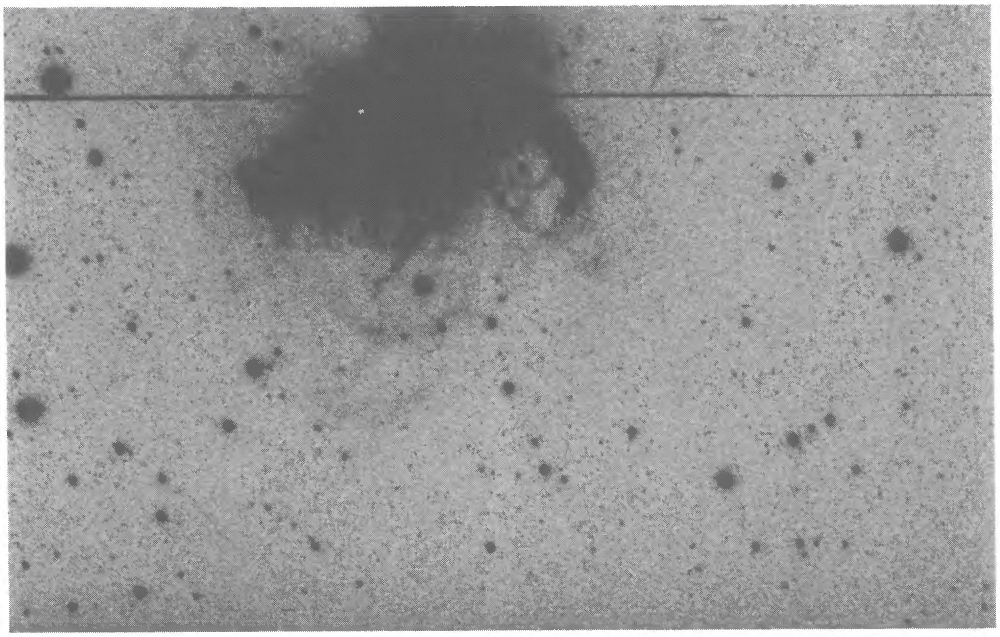

FIG. 1.—Raw CCD image of NGC 1569 taken through an Hα band filter (FWHM = 38 Å). North is up, and east is to the left. The total field of view is 7'.3 × 4'.5. Defects in the image include a row of bad pixels that passes through the galaxy and scattered light "rays" produced by the 10th mag star BD +64°450 just to the north of the field of view. All other filamentary and arclike features in the vicinity of NGC 1569 are intrinsic to the field of view and are believed to be intrinsic to the galaxy, itself.

division, and atmospheric extinction correction):

$$f_\lambda(\lambda 6500)(\text{ergs cm}^{-2}\ \text{s}^{-1}\ \text{Å}^{-1}) = 1.4 \times 10^{-17} R_0(R\ \text{band})(\text{ADU s}^{-1}) , \quad (1)$$

$$f(H\alpha)(\text{ergs cm}^{-2}\ \text{s}^{-1}) = 1.7 \times 10^{-14} R_0(\lambda 6563, \Delta\lambda 38)(\text{ADU s}^{-1}) , \quad (2)$$

$$f_\lambda(\lambda 8290)(\text{ergs cm}^{-2}\ \text{s}^{-1}\ \text{Å}^{-1}) = 1.6 \times 10^{-17} R_0(I\ \text{band})(\text{ADU s}^{-1}) , \quad (3)$$

$$f([\text{S III}])(\text{ergs cm}^{-2}\ \text{s}^{-1}) = 4.2 \times 10^{-14} R_0(\lambda 9540, \Delta\lambda 144)(\text{ADU s}^{-1}) . \quad (4)$$

Uncertainty in the derived fluxes primarily comes from the noise in the subtracted sky backgrounds. The resulting uncertainties are estimated to be $\delta I_\lambda(\lambda 6500) \approx 3.9 \times 10^{-19}$ ergs cm^{-2} s^{-1} arcsec^{-2} Å^{-1}, $\delta I(\text{H}\alpha) \approx 3.9 \times 10^{-17}$ ergs cm^{-2} s^{-1} arcsec^{-2}, $\delta I_\lambda(\lambda 8290) \approx 5.3 \times 10^{-19}$ ergs cm^{-2} s^{-1} arcsec^{-2} Å^{-1}, and $\delta I([\text{S III}]) \approx 4.1 \times 10^{-16}$ ergs cm^{-2} s^{-1} arcsec^{-2}. For the narrow-band images, the uncertainties correspond to approximately 5% of the subtracted sky value; and for the broad-band images, the uncertainties correspond to about 1% of the subtracted backgrounds.

To create an Hα image that is free from contamination by the stellar and nebular continua, an appropriately sky-subtracted, shifted, and scaled *R* band image was subtracted from the original sky-subtracted Hα band image according to the standard practices (Jacoby, Quigley, and Africano 1987; Waller 1990*a*). The scaling was determined from synthetic aperture photometry of foreground stars in the field of NGC 1569. Similar processing of the *I* band and [S III] band image was done to obtain a pure [S III] emission-line image, weak as it was. To obtain a red continuum image that is free from contamination by the Hα emission line, a scaled Hα band image was subtracted from the *R* band image, where the scaling was determined from the relative bandwidths of the Hα and *R* band filters (Waller 1990*a*).

As a check on the image processing, I have compared the Hα flux from the 3' × 3' field surrounding NGC 1569 with the flux measured photoelectrically by Kennicutt and Kent (1983) through a 3' diameter aperture. After correcting the detected flux for a 4% contamination by [N II], I derive an Hα flux of $(2.03 \pm 0.12) \times 10^{-11}$ ergs cm^{-2} s^{-1}, which is 11% lower than Kennicutt and Kent's value of $(2.26 \pm 0.33) \times 10^{-11}$ ergs cm^{-2} s^{-1}. Within the uncertainties, the two values are in good agreement.

III. MORPHOLOGIES, FLUXES, AND COLORS

Figure 2 (Plate 11) shows the Hα and red continuum images of NGC 1569 that were obtained after having subtracted off contaminating continuum emission from the Hα band image and contaminating line emission from the *R* band image. Immediately apparent is the enormous difference in emission morphologies. While the red continuum emission is dominated by a central barlike feature, the Hα emission is lumpier, off-center with respect to the stellar "bar," and far more extended at low surface brightness levels. Contour diagrams of the Hα emission (Fig. 3) and stellar continuum emission (Fig. 4) help to show these differences with even greater clarity.

a) Diffuse Hα *Emission*

The extended Hα emission is particularly striking in its similarity to the Hα plumes and filaments that emanate from the more powerful M82 starburst. Both systems of extended emission are currently thought to be the byproducts of recent eruptions from the respective nuclei. The NGC 1569 system is characterized by a bright armlike feature to the west, filamentary structures radiating outward from the north and south, and two arclike swatches of emission with large southern displacements from the nucleus. All but the last two features have been previously noted (cf. Hodge 1974; de Vaucouleurs, de

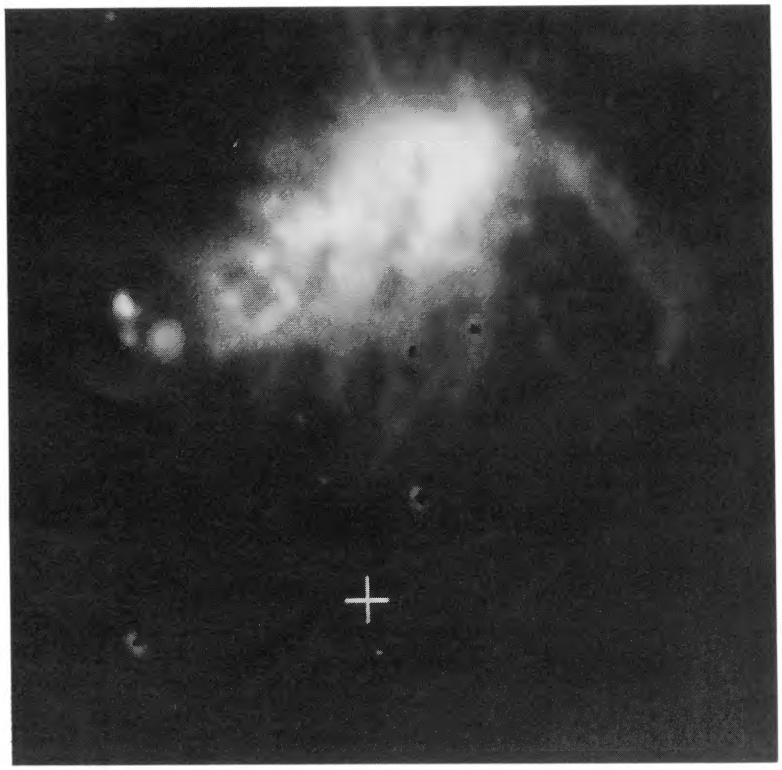

FIG. 2*a*

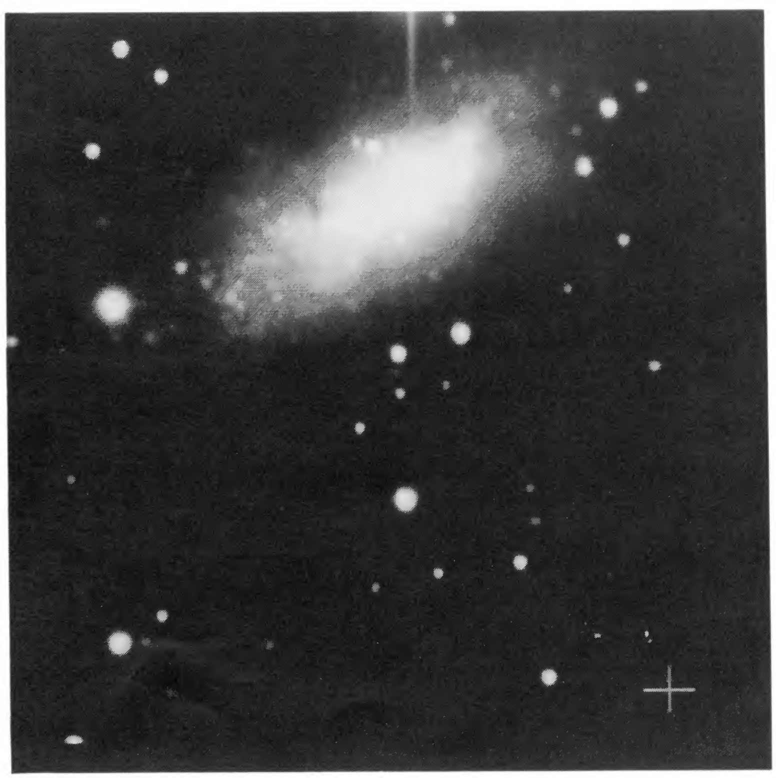

FIG. 2*b*

FIG. 2.—CCD imagery of the Hα and red continuum emission from NGC 1569. North is up, and east is to the left. The total field of view in each image is 3′ × 3′ (1.9 kpc × 1.9 kpc). Each image is a logarithmic representation of surface brightness. (*a*) NGC 1569 in the light of Hα. Continuum emission within the Hα filter bandpass has been eliminated by scaling and subtracting an *R* band image from the Hα band image. Some continuum features persist, however, including the two incompletely subtracted stars to the south and one especially bright star to the east. The western "arm" and northern and southern filaments are evident here, but the southern "arcs" are too faint to show up in this representation. (*b*) The inner "bar" of NGC 1569 at red wavelengths. Contaminating Hα emission within the *R* filter bandpass has been eliminated by scaling and subtracting an Hα band image from the *R* band image. The sharp ray to the north is due to scattered light from the bright foreground star BD +64°450 falling on the CCD chip. Individual stars are evident in the galaxy just outside of the bright central region. A dust lane is also evident in the northeast part of the bar.

WALLER (see 370, 146)

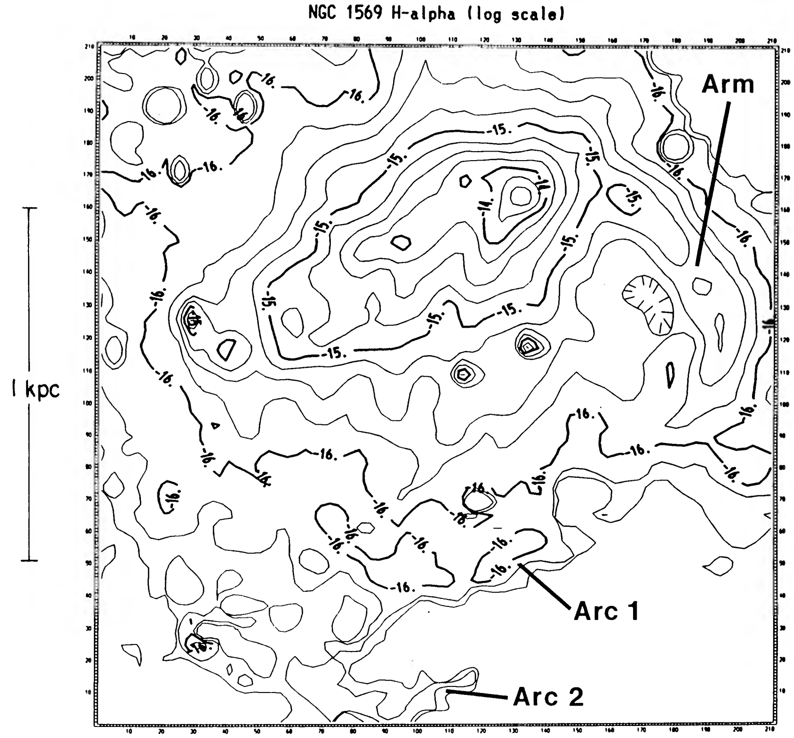

FIG. 3*a*

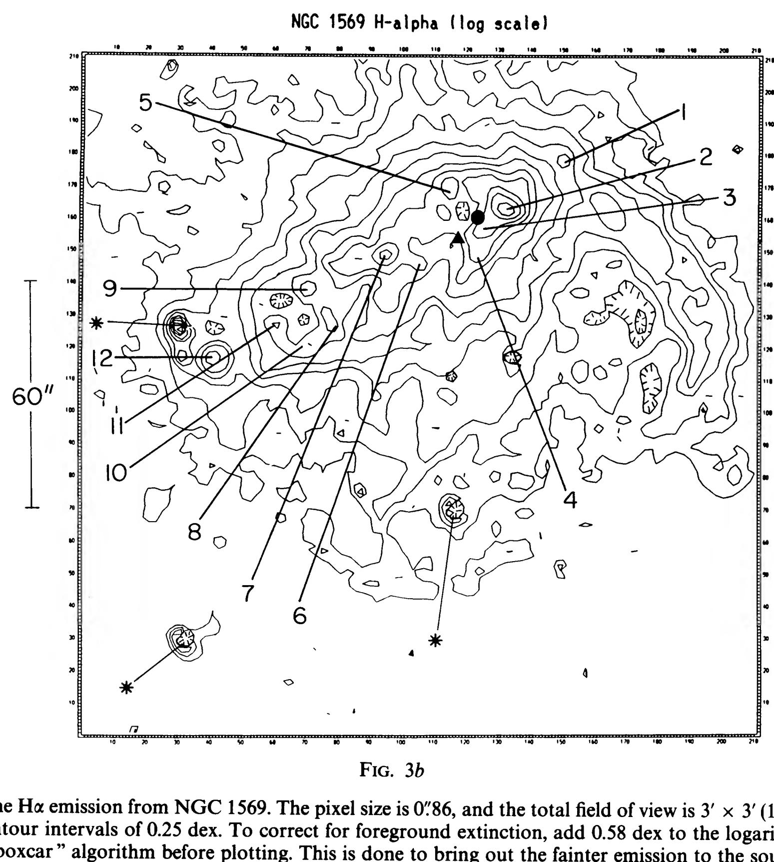

FIG. 3*b*

FIG. 3.—Contour diagrams of the Hα emission from NGC 1569. The pixel size is 0″.86, and the total field of view is 3′ × 3′ (1.9 kpc × 1.9 kpc). The Hα emission is contoured logarithmically with contour intervals of 0.25 dex. To correct for foreground extinction, add 0.58 dex to the logarithmic values. (*a*) The data have been smoothed via a 4 pixel × 4 pixel "boxcar" algorithm before plotting. This is done to bring out the fainter emission to the south. The contouring begins at the 1 σ level ($10^{-16.5}$ ergs cm^{-2} s^{-1} arcsec^{-2}) with the major logarithmic values labeled. (*b*) The data have been plotted with minimal smoothing, so that greater detail can be shown. The contouring begins at the 3 σ level (10^{-16} ergs cm^{-2} s^{-1} arcsec^{-2}). The filled circle and triangle denote the positions of objects A and B, respectively. The numbers denote the major H II regions as listed in Tables 3 and 4. Asterisks denote incompletely subtracted stars. Some filamentary structure in the diffuse emission is evident to the north and south of the brightly emitting bar.

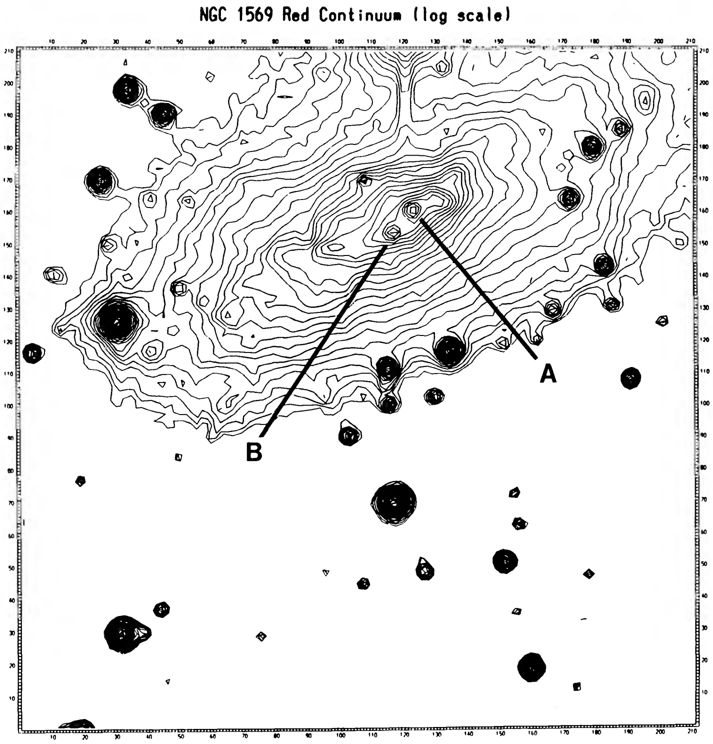

FIG. 4a

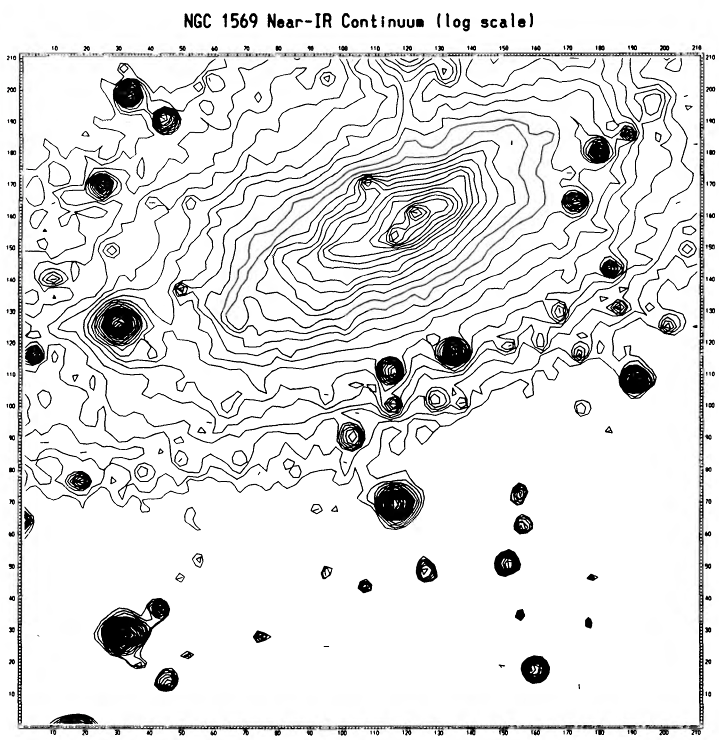

FIG. 4b

FIG. 4.—Contour diagrams of the red and near-infrared continuum emission from NGC 1569. Same field of view as before. The red (λ6500) (*a*) and near-infrared (λ8290) (*b*) continua are contoured logarithmically beginning at the 3 σ level of surface brightness (10^{-18} ergs cm^{-2} s^{-1} arcsec^{-2} Å^{-1}) with contour intervals of 0.1 dex. To correct for foreground extinction, add 0.58 dex to the logarithmic values in the λ6500 image and 0.43 dex to those in the λ8290 image. The two starlike objects near the nucleus have been labeled in accordance with Ables (1971). Scattered light from the star BD +64°450 is evident to the north of object A.

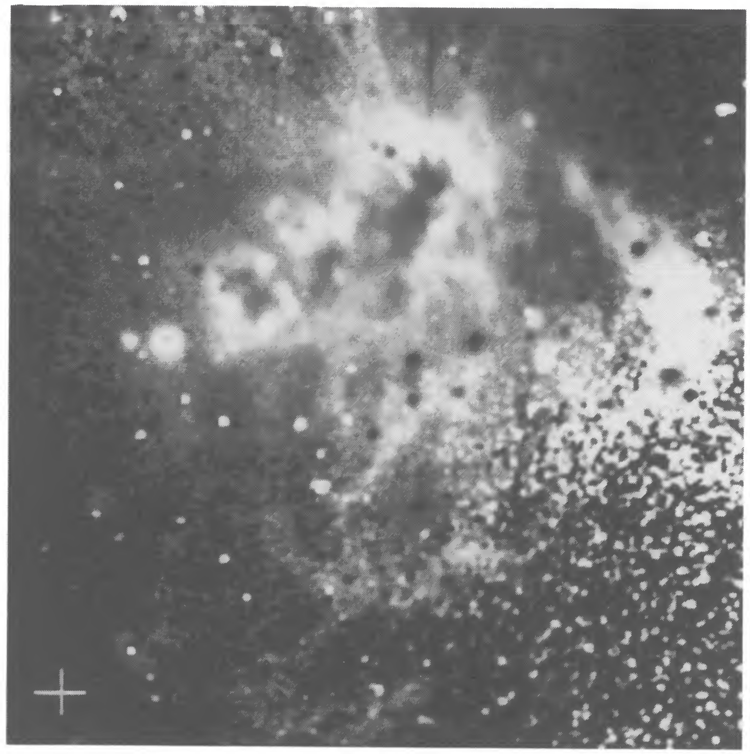

FIG. 5a

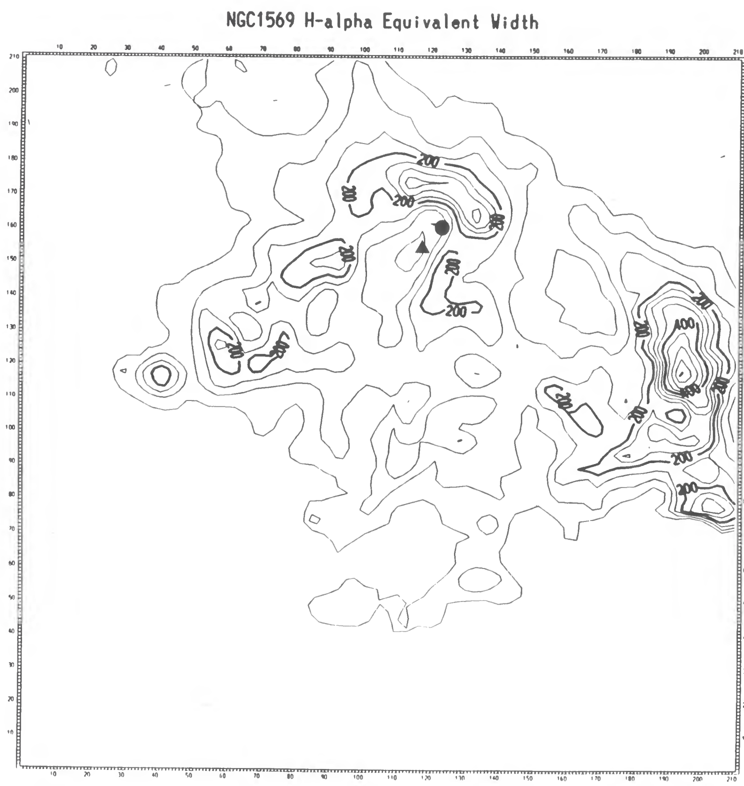

FIG. 5b

FIG. 5.—Representations of the Hα equivalent width in NGC 1569. Same field of view as before. Since it is a line-to-continuum emission ratio, the Hα equivalent width highlights regions where (1) the contrast between recent star formation and past-averaged star formation is especially strong and where (2) diffuse Hα emission with no stellar counterpart is evident. (*a*) Image of the Hα equivalent width. H II regions in the bar, the diffuse arm to the west, and the diffuse arc segments to the south are especially prominent. (*b*) Contour representation of the Hα equivalent width, showing enhancements at the locations of the H II regions, the arm, and arc 1. The contouring begins at EW(Hα) = 50 Å with contour intervals of 50 Å. The filled circle and triangle denote the positions of objects A and B, respectively.

TABLE 3

Positions and Sizes of H II Regions and Other Features

Name (1)	α(1950) (2)	δ(1950) (3)	ΔX (4)	ΔY (5)	R (6)	Identification (7)
A	$4^h26^m3^s.7$	64°44′29″	0″.0	0″.0	4″.4/1″.1	Ables
B	4 26 04 5	64 44 23	5.2	6.0	4.3/1.0	...
1	4 25 59 9	64 44 45	−24.2	15.9	(2.9)	HK(50)
2	4 26 02 4	64 44 31	−8.2	1.8	(6.4)/3.2	SB(A), HK(45)
3	4 26 03 5	64 44 26	−0.9	−3.0	(5.2)	SB(c)
4	4 26 03 7	64 44 18	−0.1	−10.7	(3.8)	HK(43)
5	4 26 04 8	64 44 35	6.8	6.4	3.4	SB(E), HK(36)
6	4 26 06 0	64 44 16	14.5	−12.5	(4.3)	HK(29)
7	4 26 07 6	64 44 19	24.8	−9.9	8.3	SB(F), HK23
8	4 26 09 6	64 44 00	37.7	−28.8	6.0	HK(11)
9	4 26 10 8	64 44 10	45.5	−19.3	5.2	HK(7)
10	4 26 10 9	64 43 55	46.3	−34.0	3.4	HK(8)
11	4 26 12 0	64 44 00	53.2	−28.8	4.5	HK(4)
12	4 26 14 5	64 43 52	69.6	−37.4	5.6	HK(2)
Arm	4 25 58 2	64 44 31	−35.1	1.9	(60 × 20)	HK(50)
Arc 1	4 26 06 1	64 42 51	15.4	−97.6	(70 × 25)	...
Arc 2	4 26 05 8	64 42 27	13.7	−121.7	(60 × 20)	...

Col. (1).—Object's designation. A and B denote the puzzling blue continuum sources near the nucleus of NGC 1569. The numbers denote Hα-emitting H II regions as identified by the author. The arm and arcs are Hα-emitting features with no corresponding enhancements in the continuum. They are therefore not *classic* H II regions with underlying star clusters.

Col. (2).—Right ascension based on the offset, ΔX, from object A and the R.A. of object A determined by Ables 1971. The position of the arm refers to its brightest part.

Col. (3).—Declination based on the offset, ΔY, from object A and the declination of object A determined by Ables 1971.

Col. (4).—Offset in right ascension from object A in the detector plane (not on the celestial sphere).

Col. (5).—Offset in declination from object A in the detector plane.

Col. (6).—Radius of object. For objects A and B, both the background-limited radius and half-width at half-maximum are given. For the H II regions (except for the brightest one), only the background-limited radius is given. Values in parentheses indicate the presence of blending by neighboring sources. For the arm and arcs, approximate dimensions are given.

Col. (7).—Cross-referenced identification of the feature. Ables refers to the optical continuum sources of Ables 1971. SB refers to the radio continuum sources of Seaquist and Bignell 1976. There is an error in this latter reference with regard to the position of SB(A). Their map shows the correct declination to be 64°44′32″. HK refers to the Hα sources identified by Hodge and Kennicutt 1983.

Vaucouleurs, and Pence 1974). Unlike the classic H II regions, the diffuse emission is not associated with any ionizing star clusters. This is most clearly shown in the map of Hα equivalent widths (i.e., line-to-continuum ratios) (Fig. 5), where the regions of diffuse emission show up as dramatic enhancements in line emission relative to the ambient continuum emission. Much of the diffuse Hα emission is spatially coincident with spur-like extensions in the diffuse H I emission (Israel and van Driel 1990, Figs. 1 and 2).

The most prominent extended feature is the western "Arm" that begins 27″ to the west of object A and curves southward for a total displacement of about 1′.1. It has projected dimensions of 640 pc × 213 pc and has an ionization requirement equivalent to 1.3×10^{51} Lyman continuum photons s^{-1} (see Tables 3 and 4). The source of this ionization could be either UV photons from hot stars in the bright central bar or energetic collisions from encounters between outflowing hot gas and cooler ambient gas. The twisted morphology that is evident in the present Hα imagery and in previous photographs (Hodge 1974), is reminiscent of the "corkscrew" structure seen by Williams, Caldwell, and Schommer (1984) in the northern plume of M82. Both structures may represent the limb-brightened "walls" that separate the hot outflowing gas from the cool neutral gas exterior to the outflow (cf. Sofue 1988). Neutral hydrogen observations of NGC 1569 seem to corroborate this picture, showing a large armlike H I feature that lies exterior to the Hα arm and which extends for more than 3′ (Reakes 1980), along with a smaller H I extension that is more closely coincident with the Hα arm (Israel and van Driel 1990).

The velocity field of the arm, as measured by de Vaucouleurs, de Vaucouleurs, and Pence (1974) and de Vaucouleurs (1981), is remarkably uniform, averaging -8 ± 5 km s^{-1} with respect to the systematic velocity of -77 km s^{-1}. If the arm represents gas flowing outward from the bar in a direction perpendicular to the inclined disk, then the measured radial velocity would correspond to a flow velocity of 18 km s^{-1}. This is less than one-tenth the flow velocity of M82's "corkscrew" as computed from similar considerations (Williams, Caldwell, and Schommer 1984). It is also barely supersonic, thus constraining the energy available for shock heating. Spectroscopic observations of collisionally excited emission lines (e.g., the [S II] (λλ6717, 6731) doublet) from this feature will be necessary, before a reliable discrimination of the ionizing source can be made.

The raylike filaments in the north and south can be traced back to a common origin that includes objects A and B. This was first noted in a sketch by de Vaucouleurs, de Vaucouleurs, and Pence (1974), based on the photographs by Hodge (1974), and is corroborated by the present CCD imagery. A strict straight-line backtracking of the filamentary trajectories results in a convergence circle 6″ in diameter located 2″.5 west of object B, but many of the filaments are obviously curved, so this should not be taken too seriously.

TABLE 4

Hα FLUXES AND EQUIVALENT WIDTHS

Name (1)	log f(Hα) (2)	EW (total) (3)	EW (cluster) (4)	log L_0(Hα) (5)	log N_i (6)
1	−13.22	121	1225	38.13	50.00
2	−11.32	304	734	40.03	51.90
3	−11.69	103	283	39.66	51.53
4	−12.22	218	(1244)	39.13	51.00
5	−12.22	213	989	39.13	51.00
6	−12.37	80	203	38.98	50.85
7	−11.67	167	1835	39.67	51.55
8	−12.42	191	608	38.93	50.80
9	−12.55	175	787	38.80	50.67
10	−12.88	258	2035	38.47	50.34
11	−12.76	222	(8443)	38.59	50.46
12	−12.91	269	859	38.44	50.31
Arm	−12.10	98	(···)	39.25	51.12
Arc 1	−12.79	61	(···)	38.56	50.43
Arc 2	−13.22	3564	(···)	38.13	50.00

COL. (1).—Object's designation. See Table 3 for cross-references.

COL. (2).—Logarithm of the Hα flux, as measured in units of ergs cm^{-2} s^{-1}.

COL. (3).—The Hα equivalent width, i.e., the line-to-continuum flux ratio, as measured in Å. The red continuum involved here includes *both* the young cluster light and the older light from the ambient galaxy.

COL. (4).—The Hα equivalent width pertaining to the ionizing cluster, in Å. The red continuum involved here includes *only* the young cluster light. Values in parentheses are uncertain due to difficulties in segregating the cluster and ambient continuum components.

COL. (5).—Logarithm of the extinction-corrected Hα luminosity, in units of ergs s^{-1}. A uniform extinction of $A_{H\alpha} = 0.81\ A_v = 2.59\ E(B-V) = 1.45$ mag has been assumed.

COL. (6).—Lyman-continuum photon production rate in units of photons s^{-1}.

The radial velocity field in the filamentary regions shows a strong gradient, with the northern filaments redshifted and the southern filaments blueshifted with respect to the systemic velocity (de Vaucouleurs 1981; note that an *oppositely directed* gradient is erroneously reported in de Vaucouleurs, de Vaucouleurs, and Pence 1974). The deviation from systematic velocity steadily rises with increasing displacement from the nucleus, reaching a maximum detected deviation of 60 km s^{-1} in the north. If the filaments represent gas flow perpendicular to the inclined disk, then the measured deviations in radial velocity correspond to a maximum outflow velocity of 132 km s^{-1}. Such an outflow velocity is roughly half of that observed in M82's filamentary system (Williams, Caldwell, and Schommer 1984).

As in M82, the velocity gradient along the minor axis of NGC 1569 can be attributed to ionized gas in polar orbits or in outflow. De Vaucouleurs, de Vaucouleurs, and Pence (1974) have modeled the motions in terms of a *biconical outflow*, whereby the Hα filaments are located on the *surfaces* of the cones—the southern filaments tracing the farside of the southern cone, and the northern filaments tracing the nearside of the northern cone.[4] The authors neglected to note that the biconical outflows would have to accelerate, or the opening angle of the cones would have to increase with distance in order for the model to fit the observations (K. H. Böhm, private communication). Either of these considerations are possible, and so the biconical outflow scenario is far from disqualified. Nowhere is there evidence for a decrease in radial velocities with increasing distance from the nucleus. This observation will be used in dating the more distant "arcs."

The faintest Hα features of a diffuse nature are the two arclike segments to the south of the nucleus. Although the innermost arc is evident on a deep Hα photograph by Hodge (1974), no mention of it has yet to appear in the literature. The outermost arc seems to have eluded detection until now. The contour diagram in Figure 3 shows both arcs to be roughly concentric, with radii of curvature consistent with a common focus near objects A and B. The innermost arc ("arc 1") has projected dimensions of approximately 747 pc × 267 pc and has an ionization budget equivalent to 2.7×10^{50} Lyman-continuum photons s^{-1}. It appears to be part of a much larger arc that includes the western arm. The outer arc ("arc 2") is significantly fainter, appearing at the 1–2 σ level in the present image. It is clearly evident in the raw Hα band CCD image, however (see Fig. 1), and thus cannot be an artifact of the image processing. It is approximately 640 pc × 214 pc in projected size and is ionized by the equivalent of 1.0×10^{50} Lyman-continuum photons s^{-1}. Arc 2 does not seem to be a part of any larger diffuse structure. If both arcs were ejected from the nucleus perpendicular to the disk, their current displacements would be 1.17 kpc and 1.46 kpc, respectively.

If the arcs are respectively tracing the near and far sides of a conical surface (in the "spirit" of de Vaucouleurs, de Vaucouleurs, and Pence 1974)—with each tracer being equidistant from the cone's apex—then that distance would be 1.34 kpc, and the opening angle of the cone would be 24°.3. Such a geomentry, however, would require the projected lengths of the arcs to be less than 570 pc at their distance from the apex, thus violating the 747 pc and 640 pc dimensions that are measured. Moreover, the near and far segments of a conical surface that is tilted 27° toward the line of sight should show *opposite* curvatures. The observed arcs are nearly concentric, however, and thus cannot represent opposite segments of the same conical surface. The arcs are more likely tracing the limb-brightened extremities of two separate "superbubbles" that were inflated along the galaxy's minor axis. The inner superbubble is the most convincing, with the arm and arc 1 comprising a large part of its rim. It is possible that the arcs are tracing different portions of the *same* superbubble. In this scenario, density inhomogeneities rather than limb brightening would account for the two separate arcs. Given the observed morphology of the arm and arcs, however, I find the limb-brightened double-bubble interpretation more plausible.

b) H II *Regions and Their Ionizing Star Clusters*

Visual inspection of the high surface-brightness portions of the Hα image shows the bar of NGC 1569 to be populated with a clutter of H II regions. The region around objects A and B is relatively devoid of such regions, but on either side of the objects—and especially to the west of them—discrete knots of Hα emission are clearly evident. Several of these knots are not round but appear more like closely nested eggs. This is most clearly evident to the north of object B near H II region 5 (see Figs. 2*a* and 3*b*). The silhouetting effects of dust lanes could be causing these distortions, by breaking up the light from a single H II region into a small gathering of luminous ovoids. Some dust lanes are evident in the continuum images, but none are coincident with the suspect dust lanes in the Hα image. Alternatively, the distorted knots and dark lanes between them may indicate the presence of a streamlining and evacuating wind, whose origin lies somewhere near objects A and B. Such a

[4] This situation would be reversed using the *corrected* velocity field of de Vaucouleurs (1981).

gas-sweeping wind would also explain the channel of diminished Hα emission to the SE of objects A and B (see Figs. 3 and 5).

Table 3 lists the prominent H II regions in NGC 1569 along with their positions, sizes, and cross-references. This list is far from complete (see Hodge and Kennicutt 1983) but represents only those H II regions, whose sizes and Hα fluxes could be measured with some degree of reliability. Table 4 lists the fluxes and equivalent widths for these objects. The Hα equivalent widths of the ionizing clusters are computed by subtracting off the continuum light of the ambient galaxy and then dividing the Hα flux by the remaining cluster light. The cluster equivalent width is sensitive to the hardness of a cluster's radiation field and hence to the cluster's stellar population at the high-mass end. The equivalent widths measured in NGC 1569 average to about (950 ± 200) Å with a dispersion of 600 Å. Similar values have been found in the outer arms of M101 (Waller 1990*b*). They imply the presence of relatively high-mass stars ($M_* \geq 40\ M_\odot$) in the ionizing clusters (A. Campbell, private communication). This inference is corroborated by the spectroscopic detection of high-excitation species such as He I (λλ5876, 6678, 7065) and [Ar III](λ7136) (Kennicutt and Kent 1983).

The brightest H II region in NGC 1569 is located 90 pc to the west of object A. Listed as source 2 in Table 3, it coincides with the strongest radio continuum source (A) mapped by Seaquist and Bignell (1976). This H II region was the only one bright enough to rise above the noise in the [S III] image. The measured [S III]/Hα flux ratio is 0.10, which, after correction for foreground reddening, amounts of f_0([S III])/f_0(Hα) = 0.07, or roughly 5 times lower than that measured in the Orion Nebula (Dennefeld and Stasinska 1983). Such a low ratio is consistent with a high-excitation, low-metallicity H II region similar to those observed in the Small Magellanic Cloud (Dennefeld and Stasinska 1983).

The Hα luminosity of the brightest H II region is 1.1×10^{40} ergs s^{-1} (after correction for Galactic foreground obscuration) which implies an ionizing luminosity of 7.9×10^{51} Lyman-continuum photons s^{-1}, or the equivalent of 790 O6 V stars (Panagia 1973). By comparison, 30 Doradus in the LMC is almost identical in Hα luminosity (ignoring internal absorption), whereas NGC 5461 in M101 is approximately 2 times more powerful (Kennicutt 1984; Waller 1990*b*). Varying considerations of distance and internal absorption will juggle these values by factors of 2–3. More important to note is that NGC 1569 is *currently* experiencing high-mass star formation on a scale comparable with the supergiant H II regions in M101.

The *total* Hα luminosity from NGC 1569 is 4.5×10^{40} ergs s^{-1} which corresponds to a Lyman-continuum luminosity of 3.4×10^{52} photons s^{-1} and an extrapolated starbirth rate of 0.4 $M_\odot$ yr^{-1} (assuming the "Extended Miller-Scalo" IMF of Kennicutt 1983). Such figures are remarkably similar to those measured in the NGC 5461 and NGC 5462 H II region *complexes* (Viallefond, Goss, and Allen 1982; Waller 1990*b*). The size of NGC 1569's active "bar" (1.1 kpc × 0.3 kpc in the plane of the sky) is also strikingly similar to the dimensions of the supergiant H II complexes in M101 and of the starburst nucleus in M82. These resemblances could be merely coincidental or, perhaps, profoundly natural consequences of some common physical process inherent to the starburst phenomenon. Further insight will require a much larger sample of starbursting regions than is considered here (cf. Balzano 1983; Kennicutt 1984; Heckman, Armus, and Miley 1987).

c) Continuum Morphology and Colors

The red continuum image shown in Figure 2 is characterized by a bright barlike structure with some indications of silhouetting dust in the northeast portion. Beyond the "bar," individual sources can be resolved. These probably include *both* compact star clusters and individual supergiant stars belonging to the galaxy. Photometry of these continuum sources is feasible with the present imagery and is being pursued (Waller and Dracobly 1991). Imaging at a smaller pixel resolution than 0".86 would be preferable for this purpose, however. A large enough sample of measured fluxes and colors would help to reveal the supergiant stars, whose fluxes could be used to calibrate the galaxy's distance (Humphreys and Aaronson 1987). This would be a tremendous improvement over the present distance determination which is based on the photographic *B* magnitude of the brightest point-like sources and on the *assumption* that they are blue supergiants (Arp and Sandage 1985).

The contour diagrams of the red and near-infrared surface brightness (Fig. 4) show a concentration of emission centered on objects A and B. This same concentration of surface brightest is also evident at 2.2 μm (Israel 1988; Waller *et al.* 1990). Ables (1971) points out that the outer B and V contours *are not* centered on A and B but are, instead, centered on a fainter region 20" to the SE of object A. Therefore, the inner concentration probably does not represent the dynamical center of the galaxy but is, instead, a relatively young assemblage of stars in orbit around the dynamical center.

The spatial distribution of (λ6500 − λ8290) color in NGC 1569 is depicted in Figure 6. Three effects are clearly visible from this mapping. The first is the excellent correspondence between the regions of bluest color and the H II regions shown in Figure 3. This strengthens the impression that *the most recent high-mass star formation is occurring exterior to the nuclear region inhabited by objects A and B*. It is worth noting in this regard that Israel and van Driel (1990) find a 180 pc diameter "hole" in the distribution of H I emission that is centered on object A.

The second effect is the reddening of the color to the northeast of the nucleus, where the *R* band image shows an apparent dust lane. The (λ6500 − λ8290) color *excess* in this region amounts to 0.25 ± 0.05 mag, or the equivalent of $A_v = 1.2 \pm 0.2$ mag. Whether this obscuration is intrinsic to NGC 1569 or of Galactic origin remains unclear.

The third effect is the reddening of the color with increasing displacement from the central "bar." Similar changes in $(B-V)$ color were observed by Ables (1971) who notes that such behavior is characteristic of Magellanic irregular galaxies. The overall redder colors in the outer galaxy are probably not tracing increasing column densities of dust. This would imply increasing column densities of H I which are not seen (Reakes 1980; Israel and van Driel 1990). Instead, the redder colors are probably tracing redder (and older) stars. This age differential is consistent with the outer starlight being off-center with respect to the inner (younger) starlight, the two populations not having yet equilibrated.

IV. KINEMATIC AGES OF THE Hα ARCS

One way to estimate the age of the nuclear starburst in NGC 1569 is to evaluate the kinematic ages of the remnant ejecta. The two arcs are especially useful for this purpose, because their large angular displacements from the nucleus provide excellent "lever arms" with which to calculate spatial displace-

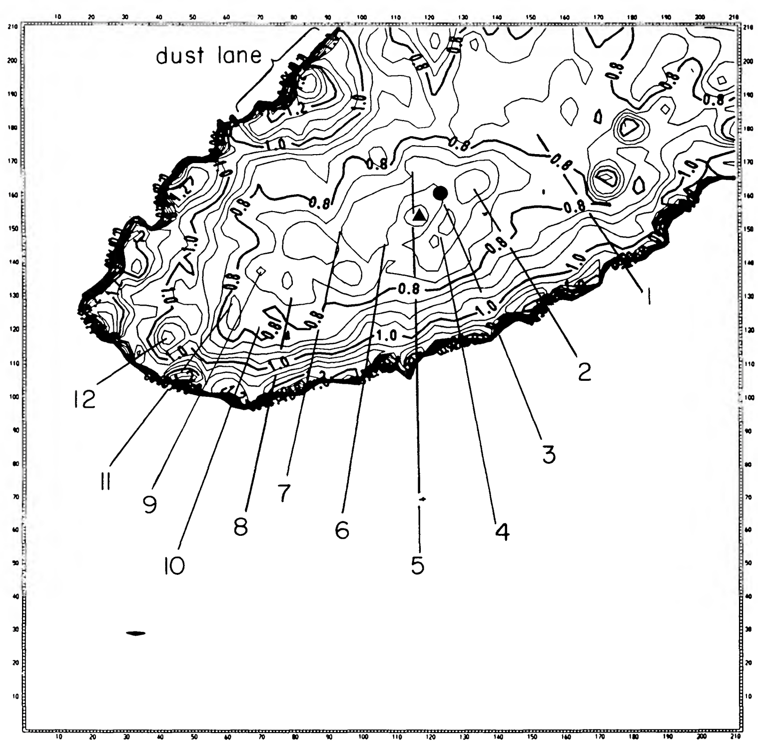

FIG. 6.—Contour diagram of the continuum color in NGC 1569. Same field of view as before. The filled circle and triangle denote objects A and B, respectively. The (λ6500 − λ8290) color within the 3 σ boundary of the corresponding red and near-infrared images is plotted with contour intervals of 0.05 mag. To correct for foreground Galactic reddening, subtract 0.38 mag from the labeled values. The bunching of contours and labels along the 3 σ boundary is an artifact of having eliminated all contouring beyond this boundary. Also note the contaminating effects caused by the scattered light from BD +64°450 located just north of the field of view. The labels indicate that the (λ6500 − λ8290) color reddens from the inside out. The bluest colors coincide with the brightest H II regions in the central bar (as noted by their corresponding numbers). The colors near the 3 σ boundary get as red as $(\lambda6500 - \lambda8290)_0 = 0.72$ mag (after correction for foreground Galactic reddening).

ments. Although the kinematic histories of the arcs are unknown, one can make some educated guesses based on the radial velocities of the filaments that are observed interior to them.

The Hα velocity field of de Vaucouleurs (1981) shows a strong gradient across the minor axis, with blueshifts in the south increasing to 40 km s^{-1} above the systemic value at a displacement of 30″ from the nucleus (the velocity field of de Vaucouleurs, de Vaucouleurs, and Pence 1974 shows the same gradient except for an erroneous change in sign.) Because the radial velocities seem to plateau at larger displacements, a first-order approximation would be to keep the velocity of the arcs constant in time and equal to the highest observed value interior to them. The apparent absence of decelerating motion and the possibility of further accelerations beyond 30″ from the nucleus suggest that the constant velocity approximation might *overestimate* the ages.

However, the orientation of the Hα arcs perpendicular to the outflow axis could be indicating that these features are tracing gas in the "snowplow" or "radiating" phase of expansion. In such a case, the expansion velocity would *decrease* as R^{-3} in a constant density medium (Tenorio-Tagle and Bodenheimer 1988 and references therein), and the constant-velocity approximation would end up yielding *underestimated* ages. In the absence of actual measurements of the velocity field out to and increasing the arcs, it is best to consider *both* expansion scenarios and so obtain lower and upper limits to the kinematic ages.

If one assumes that the arcs resulted from constant-velocity outflows along the minor axis, the 40 km s^{-1} radial velocity translates to an 88 km s^{-1} outflow velocity, and the angular displacements of the two arcs translate to 1.17 and 1.46 kpc, respectively. The resulting kinematic ages are 13.0 and 16.5 Myr, respectively. These simple estimates for the age of the nuclear starburst are well matched with the age that Israel and de Bruyn (1988) estimate based on the last major injection of energetic electrons into the ISM. Noting that the nonthermal radio emission from NGC 1569 has a high-frequency cutoff at 8 ± 1 GHz, Israel and de Bruyn ascribe the cutoff to a sharp decrease in relativistic electron injection rates about 5 Myr ago followed by synchrotron radiation losses at frequencies above 8 GHz. Their estimate for the *mean* age of the electron-injecting supernova outbursts is 10–20 Myr.

If, instead, the arcs are delineating gas that has decelerated as R^{-3}, then the kinematic ages could be up to 6 times higher than the above estimates. This follows from conserving momentum while sweeping up gas in a constant density medium, thus yielding

$$t - t_0 = \frac{(R^4 - R_0^4)}{4v_0 R_0^3}, \quad (5)$$

where t_0 is the transition time from adiabatic expansion to momentum-conserving expansion, R_0 is the radius at this transition, and v_0 is the corresponding expansion velocity. These quantities, in turn, are functions of the total mechanical energy and ambient gas density (Woltjer 1972). By adopting the energies derived from a momentum-conserving model (see § Vc) and assuming $n_i = 0.1$ cm^{-3} throughout, I obtain expansion times of 52 Myr and 68 Myr for the two arcs.

V. ENERGETICS OF THE ARCS

a) Ionization Requirements

In the absence of diagnostic spectra, it is virtually impossible to determine the source of ionization of the arcs. However, one can still estimate the Lyman-continuum production rate that hot stars near the nucleus would need to ionize these distant regions. If it is much higher than that currently measured in the brightest H II regions, then ionization by shock heating would begin to look more attractive.

For simplicity, I let the arcs be modeled as segments of spherical surfaces that are centered on the nucleus. They intercept the ionizing radiation from the nucleus according to the fractional areas that they fill. Further simplifying, I let the areas of the arcs be equal to the square of their longest dimension. The Hα fluxes from arc 1 and arc 2 imply ionization rates of 2.7×10^{50} s^{-1} and 1.0×10^{50} s^{-1}, respectively. These two rates are consistent with photoionization from a source near the nucleus, if that source has a Lyman-continuum luminosity of 8.3×10^{51} s^{-1} (to adequately illuminate arc 1) or 6.5×10^{51} s^{-1} (to adequately illuminate arc 2). These ionizing luminosities are nearly identical to that measured in the brightest H II region in the "bar" ($N_i = 7.9 \times 10^{51}$ s^{-1}). They all require the equivalent of ~ 800 O6 V stars. Therefore, the ionization requirements for the arcs can be easily provided by a population of hot stars similar to those that are ionizing the brightest H II regions. Whether this population coincides with objects A and B remains unclear, though the spectra of Arp and Sandage (1985) seem to be a little too "soft" to provide the required UV luminosity.

Ionization by shocks would require a mechanical energy output large enough to feed the diffuse Hα luminosity of $\sim 10^{40}$ ergs s^{-1} for a duration of $\sim 10^7$ yr. This amounts to $\sim 10^{54}$ ergs, which is again within the realm of possibilities (see following section). Therefore, shock wave heating and irradiation by hot stars both remain plausible ionization mechanisms, given the available data. Diagnostic spectroscopy of the arm and arcs should eventually decide the matter.

b) Gravitational and Kinetic Energies

One way to estimate the mechanical energy expended during the nuclear starburst is to estimate the gravitational and kinematic energies associated with the ejected arcs. This requires determining the masses of the arcs which, in turn, requires some knowledge of the ionized gas density. For hydrogen in ionization equilibrium, the condition of equilibrium can be stated as

$$N_i = \alpha_B n_{H^+} n_e V \, , \qquad (6)$$

where the ionization rate, N_i is determined from the Hα luminosity, the recombination coefficient of hydrogen at $T = 10^4$ K is $\alpha_B = 2.6 \times 10^{-13}$ cm^3 s^{-1} (Osterbrock 1974), and the volume, V, refers to that which is *completely filled* by the ionized gas (rather than the total volume associated with the emitting region). This statement can be rewritten in terms of the mass and density of ionized hydrogen according to

$$N_i = \frac{M_{H^+} n_{H^+} \alpha_B}{m_H} \, , \qquad (7)$$

as long as the density of free electrons is nearly equal to the density of free protons. The mass of ionized hydrogen is therefore

$$M_{H^+} = \frac{N_i m_H}{n_{H^+} \alpha_B} \, , \qquad (8)$$

where the density, n_{H^+}, refers to the density of ionized gas specific to the Hα-emitting regions rather than the density averaged over the volume of the entire emitting feature.

If observations of the density-sensitive [S II] or [O I] doublet transitions are available, it is possible to estimate the density from the measured flux ratio of one or the other flux doublet. Such observations are lacking for the diffuse emission in NGC 1569. The polar plumes in M82, however, have been observed at [S II], resulting in densities that range between 30 and 100 cm^{-3} (McCarthy, Heckman, and van Breugel 1987). Considerations of the pressure equilibrium that may operate between the H I and H II phases in NGC 1569, along with the observed H I column densities near the arcs (Reakes 1980) result in much lower densities of 0.1–1.0 cm^{-3}. These low values cannot yet be ruled out with the available data.

With the range of possible densities ranging from 0.1 to 100 cm^{-3}, the computed masses of ionized hydrogen in arc 1 and arc 2 are $8.7 \times 10^{(3-6)} M_\odot$ and $1.7 \times 10^{(3-6)} M_\odot$, respectively, the lowest exponents referring to the highest density (and lowest volume filling fraction). The corresponding gravitational energies are $2.0 \times 10^{(50-53)}$ ergs and $0.6 \times 10^{(50-53)}$ ergs, respectively. An assumed outflow velocity of 88 km s^{-1} yields kinetic energies of $10.0 \times 10^{(50-53)}$ ergs and $3.7 \times 10^{(50-53)}$ ergs, respectively.

These estimates of gravitational and kinetic energy indicate that for $n_{H^+} \sim 100$ cm^{-3}, a single supernova of energy 10^{51} ergs would be barely sufficient to eject one of the arc segments. However, lower densities would require up to 10^4 supernova explosions per arc segment. The ejection of the western arm along with arc 1 as part of a single coherent eruption would require even more energy. Inefficient coupling of the supernova energy to mechanical motions of the gas is also likely, thus increasing the energy requirements even further. Anticipated coupling efficiencies are in the 1%–5% range (Spitzer 1978), so the least amount of energy required to expel arc 1 would be equivalent to about 50 supernova explosions.

Despite the large uncertainties inherent to estimating the masses of the ionized ejecta, the computed energy requirements are sufficiently constrained to indicate that *each arc was powered by more than one supernova explosion.* The actual number of detonations per arc ranges between 10 (for arc 2 assuming $n_{H^+} = 100$ cm^{-3} and 5% coupling efficiency) and 10^5 (for arc 1 assuming $n_{H^+} = 0.1$ cm^{-3} and 1% coupling efficiency). The best guess would have $n_{H^+} \approx 1$–10 cm^{-3}, with a 3% coupling efficiency, thus yielding roughly 10^3 detonations per arc.

c) Hydrodynamic Energetics

If the arm and arcs—unlike the inner filaments—are in the "snowplow" or radiating phase of their expansion, then one can invoke momentum conservation and so estimate the *total* energy expended in the eruption(s). Given an instantaneous deposition of energy E, momentum conservation yields

$$E = 5.3 \times 10^{43} n_i^{1.12} R^{3.12} v_{\rm exp}^{1.4} \text{ ergs} \qquad (9)$$

(Tenorio-Tagle and Bodenheimer 1988 and references therein), where n_i is the preshell ambient density (in cm^{-3}), R is the average shell radius (in pc), and v_{exp} is the expansion velocity (in km s^{-1}). The expansion velocity of the arcs is set to the velocity dispersion of the ambient H I gas, which Reakes (1980) determines to be 12 ± 4 km s^{-1}. Because this is the minimum velocity that will sustain coherent structures, the resulting energy is also a lower limit. From the measured H I column densities (Reakes 1980) along with simple geometric considerations of the H I distribution, the ambient preshell density is estimated to be $n_i \approx 0.1$ cm^{-3}. The resulting energy expended is $E \approx (5.3 \pm 2.6) \times 10^{53}$ ergs for arc 1 and $(10.6 \pm 5.2) \times 10^{53}$ for arc 2, or a combined equivalent of 53,000 supernovae assuming a 3% coupling efficiency. The corresponding expansion times are 52 Myr and 68 Myr, respectively, which is about 4 times larger than that determined using the constant-velocity approximation. Increasing the arc velocities to that observed in the arm has the effect of doubling the energy output while halving the expansion times.

In the Milky Way, the estimated rate of supernova explosions is roughly one every 25 years or 40,000 per Myr. Scaling NGC 1569's supernova activity according to its smaller current ionizing star formation rate (one-tenth that of the Milky Way) produces an estimated supernova rate of 4000 per Myr. The nuclear starburst $\sim 10^7$ yr ago probably involved a significantly higher supernova rate than this. Therefore, the possibility of a coherent ($\Delta t \sim 1$ Myr) salvo of 10^3–10^4 supernovae from the nucleus producing each of the observed superbubbles is not so farfetched. Indeed, similar arguments have been used to explain the kpc-size "supershells" that are evident in 21 cm maps of the Milky Way and in deep Hα images of the LMC (Kulkarni and Heiles 1988 and references therein).

From the nonthermal radio luminosity that they measure in NGC 1569, Israel and de Bruyn (1988) estimate the total nonthermal energy content to be about 4.4×10^{54} ergs. Approximately 5×10^5 supernova remnants could account for this energy (Woltjer 1972). The corresponding supernova rate would have been about 25,000 per Myr (assuming a total burst period of 20 Myr), or about 6 times the current estimated rate. The starbirth rate would have been enhanced by the same factor, amounting to 2 $M_\odot$ yr^{-1}.

VI. DISCUSSION

a) A Starburst History

The data presented here and elsewhere seem to be converging on a common scenario for the recent history of NGC 1569. Approximately 10–60 Myr ago, the nucleus of this gas-rich dwarf experienced a sudden increase of high-mass star formation. The starburst does not seem to have been provoked by any encounters with other galaxies. The nearest large galaxy, IC 342, is more than 200 kpc away from NGC 1569, and hence has been well beyond interaction range for more than a Gyr. The possibility of an encounter with an intergalactic gas cloud (which could have fueled the burst) cannot be ruled out, however.

The starburst occurred near but not in the nucleus as defined by the isophotes of the older stellar population. The resulting stellar population currently dominates the inner galaxy at optical and near-infrared wavelengths. Associated with the center of the young stellar population are objects A and B, whose luminosities and spectra qualify them as superstar clusters, ~ 5 times brighter than the 30 Doradus cluster. Depressions in the H I and Hα emission are also coincident with this region.

The starburst created supernovae at a rate of approximately 25,000 Myr,$^{-1}$ which corresponds to a starbirth rate of about 2 $M_\odot$ yr^{-1} assuming an IMF similar to the one operating in the Milky Way. The supernovae have injected the ISM with relativistic electrons whose synchrotron emission is observed at radio frequencies. A rapid dropoff in the supernovae production rate approximately 5 Myr ago is responsible for the observed dropoff in nonthermal emission at frequencies above 8 GHz.

The supernovae have also produced massive outflows of gas along the galaxy's minor axis. Some of this gas continues to be ionized, because it is visible in the light of Hα. Photoionization from hot stars in the "bar" or collisional ionization from interactions between the outflowing gas and cooler gas in the "halo" could explain this activity. Near the bar, the outflow is characterized by raylike filaments of ionized gas which can be traced backward to a small region near objects A and B. The outflow appears to accelerate with increasing distance from the bar. Alternatively, the faster ejecta could have simply attained greater displacements.

Farther out, the interaction of the outflow with ambient gas in the halo has produced armlike pileups of Hα-emitting ionized gas and 21 cm emitting neutral gas that reach southwards from the western end of the bar. The Hα "arm" along with "arc 1" to the south appear to be limb-brightened segments of a vast bubble that was blown out by a coherent salvo of supernova detonations. Depending on the kinematic history of the ejecta, this happened between 10 and 60 Myr ago. Another eruption of supernovae occurred between 2 and 20 Myr earlier (again depending on the kinematic history of the ejecta), producing the more distant "arc 2." Thousands of supernovae were probably responsible for creating each of the observed bubble segments.

High-mass star formation continues today ($\tau \leq 5$ Myr), as evidenced by the Hα emitting H II regions and their underlying blue clusters. The H II regions are located in the bar on opposite sides of the once bursting nucleus. The most active star-forming region, located to the west of objects A and B, includes an H II region equivalent in Hα luminosity to the 30 Doradus H II region. The ongoing starbirth activity throughout the bar is strikingly similar in size, intensity, and stellar population to that seen in the supergiant H II region complexes NGC 5461 and NGC 5462 in M101. Though still impressive, the present activity is several times lower than that experienced during the heyday of the starburst. Declining activity is expected to ensue at the extremities of the bar until the nucleus cools off and fills up again with cool star-forming gas.

In its 15 Gyr lifetime, NGC 1569 could have experienced six starbursts equal in intensity to the most recent one. Each burst would have been characterized by a starbirth rate of 2 $M_\odot$ yr^{-1}, a duration of 20 Myr, and cycling time of 2 Gyr. This episodic star-forming history would have led to a lifetime-averaged starbirth rate of 0.017 $M_\odot$ yr^{-1} with a total accumulation of 16×10^7 $M_\odot$ in the form of stars and stellar remnants (see Tables 1 and 5).

b) Uncertainties and Future Directions

The scenario presented here is appealing in its self-consistency. However, major gaps exist in the picture which, once exposed, may completely alter our preception of what is going on. For starters, the intensity of the burst is poorly

TABLE 5

DERIVED PROPERTIES OF NGC 1569

A. FLUXES AND COLORS

Parameter	Value
Observed	
$f(\mathrm{H}\alpha)$	2.04×10^{-11} ergs cm^{-2} s^{-1}
$\langle \mathrm{EW(H}\alpha) \rangle$	150 Å
$\langle \lambda 6500 - \lambda 8290 \rangle$	0.75 mag
Corrected	
$f_0(\mathrm{H}\alpha)$	7.71×10^{-11} ergs cm^{-2} s^{-1}
$L_0(\mathrm{H}\alpha)$	4.51×10^{40} ergs s^{-1}
$\langle \lambda 6500 - \lambda 8290 \rangle_0$	0.37 mag

B. BIRTHRATES AND DEPLETION TIME SCALES

Parameter	Value
Lifetime Averaged	
$\langle \mathrm{MLR} \rangle_{15\,\mathrm{Gyr}}$[a]	0.01 $M_\odot$ yr^{-1}
τ(gas)	18.0 Gyr
Currently Measured	
SFR_0	0.40 $M_\odot$ yr^{-1}
MLR_0[a]	0.25 $M_\odot$ yr^{-1}
τ_0(gas)	0.64 Gyr

[a] MLR refers to the mass lockup rate in low-mass stars and stellar remnants. For the Kennicutt IMF, it is 0.63 times the star formation rate (SFR). $\langle \mathrm{MLR} \rangle_{15\,\mathrm{Gyr}}$ refers to the rate obtained from dividing a galaxy's nongaseous mass (presumed to be in the form of stars and stellar remnants) by its lifetime (presumed to be 15 Gyr).

known, being based (in the previous section) on the luminosity of the nonthermal radiation from cooling supernova remnants. Using UV, optical, and near-infrared fluxes plus the evolving models of Larson and Tinsley (1978), Israel (1988) obtains a starbirth rate during the burst of $0.3 \pm 0.1\ M_\odot\ \mathrm{yr}^{-1}$. Similarly low birthrates can be derived from the galaxy's bolometric luminosity ($L_{\mathrm{bol}} \approx 1.2 \times 10^9\ L_\odot$) using standard conversions (cf. Telesco 1988). These birthrates closely resemble the "current epoch" birthrate which I derive from the Hα luminosity. Therefore, the "major burst" $\sim 10^7$ yr ago may have been less titanic than I have painted and more like the activity of the last few million years. Such activity would still be robust enough to supply the mechanical energy implied by the observed superbubbles. The cycling time between bursts would then be more like 0.3 Gyr instead of the 2 Gyr cycling time implied by the higher starbirth rate.

The ensuing outflows of hot gas have yet to be adequately mapped in X-rays, even though a bright, resolved source was detected by the *Einstein* satellite at a position close to objects A and B (Fabbiano, Feigelson, and Zamorani 1982). Visual inspection of the IPC image reveals extended emission towards the south of the emission peak. Further X-ray mapping at higher sensitivity and angular resolution would be necessary to confirm a hot outflow in NGC 1569 similar to those observed in NGC 253 and M82.

The other gas phases are also in need of better observations. The diffuse warm ionized gas—including the arm and the arcs—has yet to be observed spectroscopically. Whether it is photo- or shock-ionized remains completely unknown. The radial velocities of the arcs also awaits spectroscopic determination. Such low surface brightness measurements, though difficult, could be crucial to finding a satisfactory solution to the overall Hα velocity field. Right now, the available data can be satisfied by *either* a bipolar outflow of suitable geometry and kinematic history or windings of ionized gas in polar orbit about the major axis.

In the starburst scenario, the outward-blowing winds and supernova eruptions should have created pile-ups of H I and H_2 gas on opposite sides of the nucleus (as appears to be the case in M82; Sofue 1988 and Waller 1990*b*). The recent 13″.4 × 14″.6 resolution H I mapping by Israel and van Driel (1990) indicates that the strongest H I emission is, in fact, displaced along the major axis on opposite sides of the "hole" surrounding object A. Higher resolution H I emission and absorption-line mapping, interferometric CO mapping (at extremely high sensitivity to offset the low CO emissivity, Young, Gallagher, and Hunter 1984), and near-infrared imaging of the shock-excited H_2 emission would go far to better delineate the various phases of the ISM near the bar.

The role of magnetic fields in shaping the extended gas has yet to be investigated. The bubble-like morphology of the Hα emission evokes possible magnetic structuring akin to the transient structures observed in the solar corona. High-resolution polarization maps of the extended radio synchrotron emission would help to show what relationship, if any, exists between the galaxy's ionized outflow and its magnetic field.

Lastly, objects A and B remain enigmatic. High-resolution imaging and spectroscopy of these compact nuclear sources should finally tell us whether they are super–star clusters, forged from the gaseous implosion that brought on the starburst, or simply foreground impostors. The *Hubble Space Telescope* will be most helpful in this regard, providing its optical aberrations can be corrected.

It is a pleasure to acknowledge the helpful comments of Karl-Heinz Böhm, Doug Brown, Alison Campbell, Paul Hodge, Judith Irwin, and Alberto Noriega-Crespo. A previous version of this paper appeared as a chapter in my Ph.D. thesis (Waller 1990*b*). I am especially grateful to my thesis advisor, Steve Strom, who provided valuable tips on observing NGC 1569 and astute guidance during the subsequent analysis.

REFERENCES

Ables, H. D. 1971, *Pub. US Naval Obs.*, 2d Ser., Vol. **20**, pt. 4, p. 61.
Arp, H. C., and Sandage, A. R. 1985, *A.J.*, **90**, 1163.
Balzano, V. 1983, *Ap. J.*, **268**, 602.
Condon, J. J. 1983, *Ap. J. Suppl.*, **53**, 459.
Dennefeld, M., and Stasinska, G. 1983, *A.J.*, **118**, 234.
de Vaucouleurs, G. 1981, *Sky and Tel.*, **62**, 406.
de Vaucouleurs, G., de Vaucouleurs, A., and Corwin, H. G. 1976, *Second Reference Catalogue of Bright Galaxies* (Austin: University of Texas).
de Vaucouleurs, G., de Vaucouleurs, A., and Pence, W. 1974, *Ap. J.* (*Letters*), **194**, L119.
Fabbiano, G., Feigelson, E., and Zamorani, G. 1982, *Ap. J.*, **256**, 397.
Heckman, T. M. Armus, L., and Miley, G. K. 1987, *A.J.*, **92**, 276.
Hodge, P. W. 1974, *Ap. J.* (*Letters*), **191**, L21.
Hodge, P. W., and Kennicutt, R. C. 1983, *A.J.*, **88**, 296.
Humphreys, R. M., and Aaronson, M. 1987, *Ap. J.* (*Letters*), **318**, L69.
Hunter, D. A., Gallagher, J. S., and Rautenkranz, D. 1982, *Ap. J. Suppl.*, **49**, 53.
Israel, F. P. 1988, *Astr. Ap.*, **194**, 24.
Israel, F. P., and de Bruyn, A. G. 1988, *Astr. Ap.*, **198**, 109.
Israel, F. P., and van Driel, W. 1990, *Astr. Ap.*, **236**, 323.
Jacoby, G. H., Quigley, R. J., and Africano, J. L. 1987, *Pub. A.S.P.*, **99**, 672.
Kennicutt, R. C. 1983, *Ap. J.*, **272**, 54.
———. 1984, *Ap. J.*, **287**, 116.

Kennicutt, R. C., and Kent, S. M. 1983, *A.J.*, **88**, 1094.
Kulkarni, S. R., and Heiles, C. 1988, in *Galactic and Extragalactic Radio Astronomy*, ed. G. L. Verschuur and K. I. Kellermann (2d ed; New York: Springer-Verlag), p. 95.
Larson, R. B., and Tinsley, B. M. 1978, *Ap. J.*, **219**, 46.
McCarthy, P. J., Heckman, T., and van Breugel, W. 1987, *A.J.*, **93**, 264.
Osterbrock, D. E. 1974, *Astrophysics of Gaseous Nebula* (San Francisco: Freeman).
Panagia, N. 1973, *A.J.*, **78**, 930.
Reakes, M. 1980, *M.N.R.A.S.*, **192**, 297.
Sandage, A. R. 1986, *Astr. Ap.*, **161**, 89.
Sandage, A. R., and Tammann, G. A. 1981, *A Revised Shapley-Ames Catalog of Bright Galaxies* (Washington, DC: Carnegie Institution).
Scheffler, H. 1982, in *Landolt-Bornstein*, New Series, Vol. **2c**, p. 46.
Seaquist, E. R., and Bignell, R. C. 1976, *Astr. Ap.*, **48**, 421.
Sofue, Y. 1988, in *Galactic and Extragalactic Star Formation*, ed. R. Pudritz and M. Fich (Dordrecht: Kluwer), p. 409.
Spitzer, L. 1978, *Physical Processes in the Interstellar Medium* (New York: John Wiley and Sons), p. 260.
Stone, R. P. S. 1977, *Ap. J.*, **218**, 767.
Telesco, C. M. 1988, *Ann. Rev. Astr. Ap.*, **26**, 343.
Tenorio-Tagle, G., and Bodenheimer, P. 1988, *Ann. Rev. Astr. Ap.*, **26**, 145.
Tully, R. B., and Fisher, J. R. 1987, *Nearby Galaxies Atlas* (Cambridge: Cambridge University Press).
Viallefond, F., Goss, W. M., and Allen, R. J. 1982, *Astr. Ap.*, **115**, 373.
Waller, W. H. 1990*a*, *Pub. A.S.P.*, in press.
———. 1990*b*, Ph.D. thesis, University of Massachusetts.
Waller, W., DePoy, D., Gurwell, M., Tamura, M., and Ward, M. 1991, in preparation.
Waller, W. H., and Dracobly, C. 1991, in preparation.
Williams, T. B., Caldwell, N., and Schommer, R. A. 1984, *Ap. J.*, **281**, 579.
Woltjer, L. 1972, *Ann. Rev. Astr. Ap.*, **10**, 129.
Young, J. S., Gallagher, J. S., and Hunter, D. A. 1984, *Ap. J.*, **276**, 476.
Zwicky, F. 1971, *Catalogue of Selected Compact Galaxies and Post-Eruptive Galaxies* (Zurich: Speich).

William H. Waller: Astronomy Department, FM-20, University of Washington, Seattle, WA 98195
[BITNET: waller@phast.phys.washington.edu]